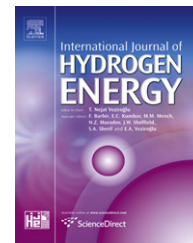Available online at www.sciencedirect.com

SciVerse ScienceDirect

journal homepage: www.elsevier.com/locate/he

Nanoconfined 2LiBH₄–MgH₂–TiCl₃ in carbon aerogel scaffold for reversible hydrogen storage

Rapee Gosalawit-Utke [a,b,*], Chiara Milanese [c], Payam Javadian [d], Julian Jepsen [a], Daniel Laipple [a], Fahim Karmi [a], Julián Puszkiel [a], Torben R. Jensen [d], Amedeo Marini [c], Thomas Klassen [a], Martin Dornheim [a]

[a] Institute of Materials Research, Materials Technology, Helmholtz-Zentrum Geesthacht, Geesthacht 21502, Germany
[b] School of Chemistry, Institute of Science, Suranaree University of Technology, Nakhon Ratchasima 30000, Thailand
[c] Pavia Hydrogen Lab., C. S. G. I., Department of Chemistry, Physical Chemistry Division, University of Pavia, Pavia 27100, Italy
[d] Center for Energy Materials, iNANO and Department of Chemistry, University of Aarhus, Aarhus C8000, Denmark

ARTICLE INFO

ABSTRACT

Nanoconfinement of 2LiBH₄–MgH₂–TiCl₃ in resorcinol–formaldehyde carbon aerogel scaffold (RF–CAS) for reversible hydrogen storage applications is proposed. RF–CAS is encapsulated with approximately 1.6 wt. % TiCl₃ by solution impregnation technique, and it is further nanoconfined with bulk 2LiBH₄–MgH₂ via melt infiltration. Faster dehydrogenation kinetics is obtained after TiCl₃ impregnation, for example, nanoconfined 2LiBH₄–MgH₂–TiCl₃ requires ~1 and 4.5 h, respectively, to release 95% of the total hydrogen content during the 1st and 2nd cycles, while nanoconfined 2LiBH₄–MgH₂ (~2.5 and 7 h, respectively) and bulk material (~23 and 22 h, respectively) take considerably longer. Moreover, 95–98.6% of the theoretical H₂ storage capacity (3.6–3.75 wt. % H₂) is reproduced after four hydrogen release and uptake cycles of the nanoconfined 2LiBH₄–MgH₂–TiCl₃. The reversibility of this hydrogen storage material is confirmed by the formation of LiBH₄ and MgH₂ after rehydrogenation using FTIR and SR-PXD techniques, respectively.

1. Introduction

Nanostructuring based on size reduction of the solid-state metal or complex hydrides for reversible hydrogen storages is currently of interest. Several research groups have revealed that the nanoscale significantly affects the hydrogen exchange kinetics and thermodynamic destabilization of hydride materials [1–5]. The high-energy ball milling technique is conventionally used to decrease the crystallite size and allow catalytic doping of inorganic materials [3,6]. Nanoparticles of various

hydride materials (with and without additives), such as metal hydrides (e.g., MgH₂–TiH₂ [7,8]), complex hydrides (e.g., LiBH₄-oxide additives [9] and LiBH₄–Mg [10]), and reactive hydride composites (e.g., 2LiBH₄–MgH₂ [3,11] and 2LiBH₄–MgH₂-transition metal chlorides [12]), have been ball milled for reversible hydrogen storage applications. Nevertheless, repeated hydrogen release and uptake cycles at elevated temperatures result in grain growth and particle agglomeration [13]. In this regard, to keep the hydride particles at nanosizes during de-/rehydrogenation cycles, nanoporous carbon aerogel scaffolds

have been recently used for hydride confinements due to their chemical inertness, light weight, and controllable pore size.

Confinement of metal hydride, e.g., MgH_2, in nanoporous carbon hosts, was carried out by various means, such as the melt infiltration of metallic Mg into Ni- or Cu-deposited carbon scaffold and hydrogenation of Mg to MgH_2 [14]. In addition, encapsulation of magnesium dibutyl ($MgBu_2$) precursor in carbon aerogel by solution impregnation and hydrogenation ($p(H_2) = 50$ bar and $T = 170\ °C$) to MgH_2 was also reported elsewhere [15,16]. Nanoconfined MgH_2 revealed a significant improvement in hydrogen sorption kinetics as compared with bulk MgH_2. For instance, MgH_2 infiltrated in Ni-deposited carbon aerogel released hydrogen at an average rate of 25 wt. % h^{-1}, while that of ball-milled MgH_2 with graphite was 0.12 wt. % h^{-1} [14]. Not only metal hydrides, but also complex hydrides have been infiltrated in nanoporous carbon aerogels, and they presented superior kinetics as compared with ball-milled materials. Nanoconfined $NaAlH_4$ prepared by melt infiltration showed a single-step dehydrogenation at low temperatures as well as rehydrogenation at mild condition (e.g., 24 bar H_2 at 150 °C) [17]. Besides, a lot of attention has been focused on the confinement of $LiBH_4$ in nanoporous carbon aerogel scaffold, due to its high gravimetric H_2 storage capacity (18.5 wt. %) [5]. Simultaneously, nanoconfinements of reactive hydride composites (e.g., $2LiBH_4$–MgH_2 [4,18,19], $2NaBH_4$–MgH_2 [20], and $LiBH_4$–$Ca(BH_4)_2$ [21]) have also been carried out. All of them showed a considerable improvement in hydrogen sorption kinetics. For example, nanoconfined $2LiBH_4$–MgH_2 in resorcinol–formaldehyde carbon aerogel released hydrogen ten times faster than the bulk sample during the 1st dehydrogenation [4]. Moreover, instead of a normal two-step dehydrogenation, a single-step reaction was obtained from $2LiBH_4$–MgH_2 after nanoconfinement, suggesting that the thermodynamics had changed [4,18]. Furthermore, catalytic doping in the nanoconfined hydride sample was performed to improve its kinetic properties. Nielsen et al. [22] reported that nanoconfinement of $NaAlH_4$ in carbon aerogel catalysed with 3.0 wt. % $TiCl_3$ showed superior dehydrogenation kinetics over both nanoconfined $NaAlH_4$ (without catalyst) and bulk $NaAlH_4$–$TiCl_3$.

On the basis of $2LiBH_4$–MgH_2 composite, it is well known that various additives, such as $TiCl_3$, $ZrCl_4$, VCl_3 [12,23], TiO_2 [24], and Nb_2O_5 [25] have been loaded to optimize the reaction performance during de-/rehydrogenation. In the present study, we extend our previous research by focussing on kinetic improvement of the nanoconfined $2LiBH_4$–MgH_2 in carbon aerogel scaffold by catalytic doping. Prior to melt infiltration of $2LiBH_4$–MgH_2, titanium trichloride ($TiCl_3$) is impregnated in carbon aerogel scaffold prepared from resorcinol–formaldehyde (RF) aerogel. Nanoconfinements of both hydride composite and catalyst are confirmed by N_2 adsorption–desorption measurements, scanning electron microscopy (SEM), and energy dispersive X-ray spectroscopy (EDS). Dehydrogenation, reversibility, reaction mechanisms, and kinetics of both nanoconfined samples (with and without $TiCl_3$) are determined by *in situ* synchrotron radiation powder X-ray diffraction (SR-PXD), Fourier transform infrared spectroscopy (FTIR), coupled manometric–calorimetric measurements, and titration experiments.

2. Experimental details

2.1. Sample preparation

The powder samples of 4.52 g $LiBH_4$ (90+ % hydrogen-storage grade, Aldrich) and 2.67 g MgH_2 (hydrogen-storage grade, Aldrich) were milled in a 2:1 mol ratio using a Fritsch Pulverisette 6 classic line planetary mill under an argon atmosphere in a glove box. The mixture was milled in a stainless steel vial (Evico Magnetic, Germany) with a ball-to-powder weight ratio (BPR) of 10:1. Milling was performed for 5 h at 400 rpm to obtain bulk $2LiBH_4$–MgH_2.

Resorcinol–formaldehyde (RF) aerogels were prepared according to the previous procedures [5,26]. The aerogel was synthesized by mixing 41.4286 g of resorcinol (99%, Aldrich), 56.64 mL deionized water, 56.92 mL of a 37 wt. % formaldehyde in a water solution stabilized by 10–15 wt. % methanol, and 0.0337 g of Na_2CO_3 (Aldrich, 99.999%) in a beaker under continuous stirring until homogeneity. The polymer solution was poured into polypropylene bottles and sealed with the lids. The solution was aged at room temperature for 24 h, at 50 °C for 24 h, at 90 °C for 72 h, and cooled to room temperature in ambient condition. The aerogel obtained was soaked in an acetone bath three times within a period of 3–4 days and dried at room temperature for several days inside the fume hood. The monolith of gels was cut into smaller pieces of ca. 0.4 cm^3 for further carbonization. The pieces of monolithic aerogel were carbonized in a tubular oven at a constant temperature of 800 °C (heating rate of 2.6 °C/min) for 6 h under nitrogen flow. The furnace was turned off, and the samples were left to cool to room temperature. The gel obtained was dried at 500 °C under vacuum for 16 h to achieve an RF carbon aerogel scaffold, denoted as RF–CAS.

The impregnation of titanium trichloride ($TiCl_3$) (>99.99% hydrogen-storage grade, Aldrich) in RF–CAS was carried out by (i) dissolving 0.0406 g $TiCl_3$ in 30 mL dried acetone (≥99.9%, Aldrich) to obtain 5.4 wt. % $TiCl_3$ solution; (ii) immersing 1.1636 g RF–CAS in $TiCl_3$ solution; and (iii) drying RF–CAS at room temperature in a glove box for several days. As the acetone evaporated, 1.1822 g of $TiCl_3$-impregnated RF–CAS (1.6 wt. % $TiCl_3$ in RF–CAS) was obtained and denoted as $TiCl_3$–RF–CAS. The bulk $2LiBH_4$–MgH_2 was ground with $TiCl_3$–RF–CAS at a weight ratio of 1:2 in the mortar. Nanoconfinement was carried out by using a Sievert-type apparatus (a PCTPro-2000 from Hy-Energy LLC). The mixture of bulk $2LiBH_4$–MgH_2 and $TiCl_3$–RF–CAS was heated to 310 °C (5 °C/min) under a hydrogen pressure of 60 bar, kept at 310 °C for 30 min, and cooled to room temperature. The sample was denoted as nanoconfined $2LiBH_4$–MgH_2–$TiCl_3$. For comparison, the nanoconfined $2LiBH_4$–MgH_2 without catalyst (1:2 weight ratio of bulk $2LiBH_4$–MgH_2: RF–CAS) was also prepared by the same procedures.

2.2. Characterizations

To characterize the texture parameters of the RF–CAS, $TiCl_3$–RF–CAS, and nanoconfined $2LiBH_4$–MgH_2–$TiCl_3$, N_2 adsorption–desorption measurements were carried out using a Nova 2000e surface area and pore size analyser from

Quantachrome. Prior to the measurements, a known amount of sample was degassed at 200 °C under vacuum for several hours. All samples were measured with a full adsorption and desorption isotherm in the pressure range of 0–1 p/p_0 at liquid nitrogen temperatures with nitrogen gas as an adsorbent. The measurement was programmed to continuously change the pressure ratio to 1 for adsorption, and to 0 for desorption. Data were analysed by the t-plot method [27,28], the Brunner Emmet Teller (BET) method [29], and the Barret Joyner Halenda (BJH) method, and the highest point of the isotherm measurement (where $p/p_0 \sim 1$) was used to calculate the total volume of the sample [30].

Scanning electron microscopy (SEM) and energy dispersive X-ray spectroscopy (EDS) were done by using an Auriga instrument from Zeiss, Germany and apparatus from EDAX Inc., USA, respectively. Smart SEM and EDS Genesis programs were used for morphological studies and elemental analysis, respectively. The powder samples were deposited onto the sample holder by using silver glue (in n-butylacetate) and continuously coated by palladium–gold sputtering with a current of 30 mA for 30 s under vacuum. An internal view of the nanoconfined $2LiBH_4$–MgH_2–$TiCl_3$ ($20 \times 20 \times 6~\mu m^3$) was produced by the focus ion beam (FIB) technique using a Canixon instrument from Orsay Physics, France. The specimen was irradiated by a gallium ion beam with an energy of 30 kV.

Coupled manometric–calorimetric measurements of nanoconfined $2LiBH_4$–MgH_2–$TiCl_3$ and $2LiBH_4$–$MgBu_2$ were carried out by connecting a high-pressure calorimeter (a Sensys DSC, Setaram) to a Sievert-type apparatus (a PCTPro-2000, Setaram & Hy-Energy). The high-pressure cell of the calorimeter, connected to the manometric instrument by a 1/8 in. stainless steel tube, was loaded with $\sim$13–25 mg of the powder samples in the glove box. Dehydrogenations were performed by heating the samples from room temperature up to 500 °C with heating rates of 5 °C/min under 3 bar H_2 pressure. The calorimetric profiles were compiled by a Calisto software to obtain the peak temperatures.

The kinetic properties concerning dehydrogenation, rehydrogenation and cycling efficiency were studied by a carefully calibrated Sievert-type apparatus (a PCTPro-2000 from Hy-Energy LLC). The powder samples ($\sim$120 mg) were put into a high pressure–temperature vessel and transferred to the Sievert-type apparatus. Dehydrogenation of nanoconfined $2LiBH_4$–MgH_2–$TiCl_3$ was done at 425 °C (5 °C/min) under $\sim$ 3.4 bar H_2. For rehydrogenation, the dehydrogenated powder was heated to 425 °C (5 °C/min) under hydrogen pressure in the range of 130–145 bar and kept at 425 °C for 12 h. For comparison, nanoconfined $2LiBH_4$–MgH_2 without catalyst was also dehydrogenated and rehydrogenated by similar procedures.

In situ synchrotron radiation powder X-ray diffraction (SR-PXD) experiments were carried out at the MAX II Synchrotron, beamline I711 in the MAX-lab Research Laboratory, Lund, Sweden [31]. The powder diffraction patterns were recorded by a MAR165 CCD detector with a selected X-ray wavelength of 0.99917 Å. The sapphire capillaries were filled airtight with the powder samples under a purified argon atmosphere in the glove box. After infiltration, dehydrogenation, and rehydrogenation, the powder samples of nanoconfined $2LiBH_4$–MgH_2–$TiCl_3$ were investigated by performing single scan X-ray diffraction. The infiltrated powder sample was dehydrogenated by heating to 435 °C (3 °C/min) under 3.5 bar H_2, kept at 435 °C for 1 h, and cooled to room temperature. In the case of rehydrogenation, the dehydrogenated powder sample was heated to 435 °C (3 °C/min) under 100–120 bar H_2, kept at 435 °C for 1 h, and cooled to room temperature.

The powder samples of nanoconfined $2LiBH_4$–MgH_2–$TiCl_3$ (after rehydrogenation) and pristine $LiBH_4$ were identified by Fourier transform infrared (FTIR) spectroscopy using a Bruker Equinox 55. The mixture of sample powder and anhydrous KBr was ground in the mortar with a weight ratio of 10:1 (KBr: powder sample), and continuously pressed under a specific pressure to obtain a KBr pellet. The KBr pellet containing the sample was placed in the sample holder assembled in the direction of infrared radiation. The spectra were collected in the wavenumber range of 3000–450 cm^{-1} with 64 scans for both sample and background.

3. Results and discussion

3.1. Nanoconfinement of composite hydride $2LiBH_4$–MgH_2 and $TiCl_3$

To confirm the successful confinement of composite hydride $2LiBH_4$–MgH_2 and $TiCl_3$ in the nanoporous structure of RF–CAS, N_2 adsorption–desorption analysis was carried out. In this study, RF–CAS with a surface area, a pore diameter, and a total pore volume of 659 m^2/g, 26 nm, and 1.30 mL/g, respectively, was used (Table 1). After impregnation of $TiCl_3$, the surface area and microporous (pore size < 2 nm) volume of the RF–CAS decrease to 629.6 m^2/g and 0.17 mL/g, respectively ($TiCl_3$–RF–CAS in Table 1). In contrast, the pore diameter and mesoporous (2 nm < pore size <50 nm) volume of $TiCl_3$–RF–CAS increase to 30.34 nm and 1.17 mL/g, respectively. This implies that $TiCl_3$ is successfully impregnated only in the microporous structure of RF–CAS. In the case of nanoconfined $2LiBH_4$–MgH_2–$TiCl_3$, significant decreases in the surface area and total pore volume to 43.5 m^2/g and 0.41 mL/g, respectively, with respect to $TiCl_3$–RF–CAS are achieved, confirming the nanoconfinement of $2LiBH_4$–MgH_2 in

Table 1 – Texture parameters of RF–CAS, $TiCl_3$–RF–CAS, and nanoconfined $2LiBH_4$–MgH_2–$TiCl_3$.

Samples	S_{BET} (m^2/g)	D_{max} (nm)	V_{micro} (mL/g)	V_{meso} (mL/g)	V_{total} (mL/g)
RF–CAS	659.0	26.0	0.19	1.10	1.30
$TiCl_3$–RF–CAS	629.6	30.3	0.17	1.17	1.35
Nanoconfined $2LiBH_4$–MgH_2–$TiCl_3$	43.5	30.1	0	0.45	0.41

TiCl$_3$–RF–CAS (Table 1). Furthermore, the SEM–EDS experiments and FIB technique were also used to investigate the states of both 2LiBH$_4$–MgH$_2$ and TiCl$_3$ in RF–CAS. Fig. 1(A) reveals the surface morphology of nanoconfined 2LiBH$_4$–MgH$_2$–TiCl$_3$, where the EDS results (Fig. 1(B)) show that most of the components are carbon (C) and oxygen (O) from RF–CAS and oxidation in air, respectively. Moreover, small amounts of magnesium (Mg) and gold (Au) representing MgH$_2$ and palladium–gold spattering, respectively, are detected. To confirm the nanoconfinement of both 2LiBH$_4$–MgH$_2$ and TiCl$_3$ in RF–CAS, a specimen of nanoconfined sample was irradiated by a gallium ion beam using the FIB technique to explore the internal areas of the RF–CAS matrices (Fig. 1(C)). From the EDS results of the area in the red frame (Fig. 1(C)), C and O are still the main elements as found on the surface, together with Mg and gallium (Ga) from MgH$_2$ and Ga-ion (FIB technique), respectively (Fig. 1(D)). However, it should be noted that the exposure of chlorine (Cl) and Ti signals (Fig. 1(D)) verifies that TiCl$_3$ is successfully impregnated in the porous structure of RF–CAS. Fig. 1(B) and (D) assure the presence of MgH$_2$ both on the surface and in the pores of RF–CAS. Due to the limitation of the EDS experiment, which is not sensitive to light elements, the existences of lithium (Li) and boron (B) from LiBH$_4$ cannot be detected. Nevertheless, the nanoconfinement of LiBH$_4$ in RF–CAS is confirmed afterwards by the SR-PXD results (Fig. 5).

The amount of each component in nanoconfined samples with and without TiCl$_3$ was also calculated by the weight difference before and after confinement. Table 2 shows that nanoconfined 2LiBH$_4$–MgH$_2$ contains 66.5, 20.7, and 12.8 wt. %

of RF–CAS, LiBH$_4$, and MgH$_2$, respectively, while nanoconfined 2LiBH$_4$–MgH$_2$–TiCl$_3$ has 65.1, 21.0, 12.3, and 1.6 wt. % of RF–CAS, LiBH$_4$, MgH$_2$, and TiCl$_3$, respectively. The mole ratios of LiBH$_4$:MgH$_2$ of both the nanoconfined samples are approximately 2:1. Regarding the dehydrogenation mechanism of 2LiBH$_4$–MgH$_2$ (Reaction (1)), 11.43 wt. % H$_2$ is reversible. Therefore, theoretical hydrogen storage capacities of 3.83 and 3.80 wt. % H$_2$ are calculated for nanoconfined 2LiBH$_4$–MgH$_2$ and 2LiBH$_4$–MgH$_2$–TiCl$_3$, respectively (Table 2).

$$2LiBH_{4(l)} + MgH_{2(s)} \leftrightarrow 2LiH_{(s)} + MgB_{2(s)} + 4H_{2(g)} \tag{1}$$
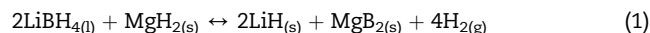
3.2. Dehydrogenation profiles

The dehydrogenation behaviours of nanoconfined samples both with and without TiCl$_3$ were studied by coupled manometric–calorimetric measurements. Fig. 2(A) and (B) show the polymeric phase transformations of the nanoconfined samples at 105 °C. For melting of LiBH$_4$, nanoconfined 2LiBH$_4$–MgH$_2$ reveals an endothermic peak at 270 °C. In the case of nanoconfined 2LiBH$_4$–MgH$_2$–TiCl$_3$, the onset temperature at ∼250 °C belongs not only to LiBH$_4$ melting, but also to partial dehydrogenation, as indicated by the reduction of the manometric response. By heating the samples, nanoconfined 2LiBH$_4$–MgH$_2$ releases hydrogen in the temperature range of 275–383 °C (Fig. 2(A)), while that of the nanoconfined 2LiBH$_4$–MgH$_2$–TiCl$_3$ begins at 250 °C, together with LiBH$_4$ melting as mentioned above, and completes at 396 °C
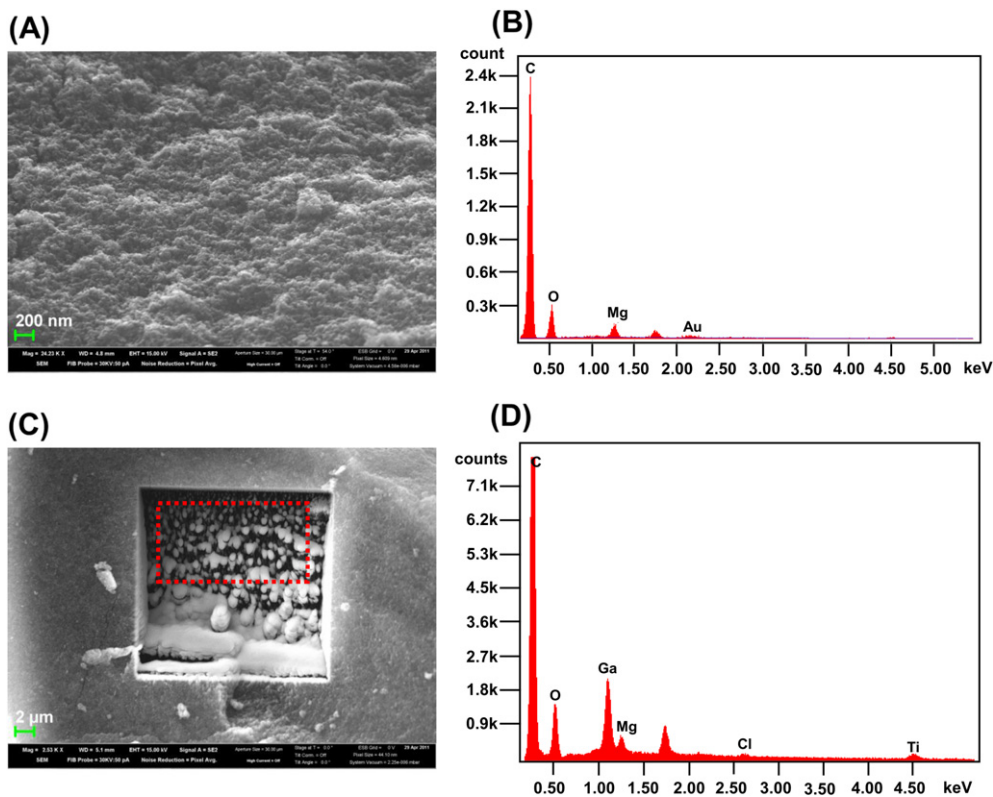

Fig. 1 – SEM micrographs and elemental analysis (EDS results) of the nanoconfined 2LiBH$_4$–MgH$_2$–TiCl$_3$ on the surface areas (A) and (B), respectively, and in the internal areas (in the red frame) (C) and (D), respectively. (For interpretation of the references to colour in this figure legend, the reader is referred to the web version of this article.)

Table 2 — Calculated amounts of all components, LiBH₄:MgH₂ mole ratio, and theoretical hydrogen storage capacities of the nanoconfined samples.

Nanoconfined samples	Amount of components (wt. %)				Molar ratio of $LiBH_4$:MgH_2	Theoretical H_2 storage capacities (wt. % H_2)
	RF—CAS	$LiBH_4$	MgH_2	$TiCl_3$		
$2LiBH_4$—MgH_2—RF	66.5	20.7	12.8	—	2:1	3.83
$2LiBH_4$—MgH_2—$TiCl_3$	65.1	21.0	12.3	1.6	2:1	3.80

(Fig. 2(B)). The manometric results of both nanoconfined samples present single-step dehydrogenation (Fig. 2(A) and (B)), corresponding to the previous studies of nanoconfined $2LiBH_4$—MgH_2 in RF—CAS with 31 nm pore size [4]. Compared with ball-milled $2LiBH_4$—MgH_2—1 mol % $TiCl_3$ sample, showing an onset temperature of 300 °C for dehydrogenation [12], it can be remarked that the dehydrogenation temperature decreases by 50 °C after nanoconfinement (nanoconfined $2LiBH_4$—MgH_2—$TiCl_3$ starts desorption at 250 °C). The amount of hydrogen released from the nanoconfined samples of $2LiBH_4$—MgH_2 and $2LiBH_4$—MgH_2—$TiCl_3$ are 3.35 and 3.58 wt. % H_2, respectively, approaching the theoretical hydrogen storage capacities (Table 2). Although the hydrogen desorption of nanoconfined $2LiBH_4$—MgH_2—$TiCl_3$ completes at a higher temperature (396 °C) than that of nanoconfined $2LiBH_4$—MgH_2 (383 °C), it starts to desorb hydrogen at a lower temperature

(250 °C). Furthermore, it should be noted that in the same desorption temperature range (room temperature to ∼500 °C), nanoconfined $2LiBH_4$—MgH_2—$TiCl_3$ releases 94.2% of the theoretical H_2 storage capacity (3.58 wt. % H_2), while that of nanoconfined $2LiBH_4$—MgH_2 gives only 87.5% (3.35 wt. % H_2). This faster dehydrogenation rate in the same temperature range suggests kinetic improvement after $TiCl_3$ impregnation.

3.3. Kinetic properties and hydrogen storage capacity

The kinetics, reversibility, and hydrogen reproducibility were evaluated using a Sievert-type apparatus. Four hydrogen release ($T = 425$ °C, $p(H_2) = 3.4$ bar) and uptake ($T = 425$ °C, $p(H_2) = 130–145$ bar) cycles were carried out on both nanoconfined $2LiBH_4$—MgH_2 and $2LiBH_4$—MgH_2—$TiCl_3$. The hydrogen back pressure (3.4 bar) used during dehydrogenation was to avoid the formation of an intermediate $Li_2B_{12}H_{12}$ phase and to encourage MgB_2 formation, considered to be crucial for the reversibility of a $2LiBH_4$—MgH_2 based system (Reaction (1)) [32]. Moreover, at least 3 bar H_2 is required to suppress the individual decomposition of $LiBH_4$ before the occurrence of Reaction (1) to produce LiH and MgB_2. However, the higher the hydrogen back pressure, the lower the dehydrogenation rate. Therefore, a hydrogen back pressure between 3 and 4 bar was used. Fig. 3 shows that both nanoconfined samples have comparable H_2 storage capacities of ∼3.6 wt. % H_2 (10.8 wt. % H_2 with respect to the hydride content) during the 1st dehydrogenation. The amount of hydrogen desorbed from both nanoconfined samples during the 1st cycle approaches the theoretical values (Table 2) and those from manometric—calorimetric results (Fig. 2). Moreover, it should be noted that desirable kinetics is
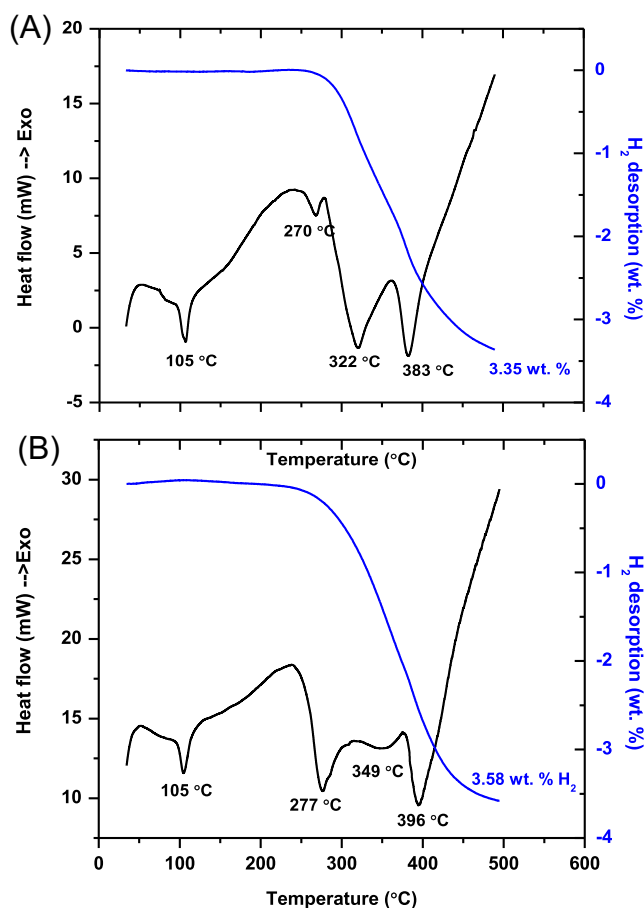

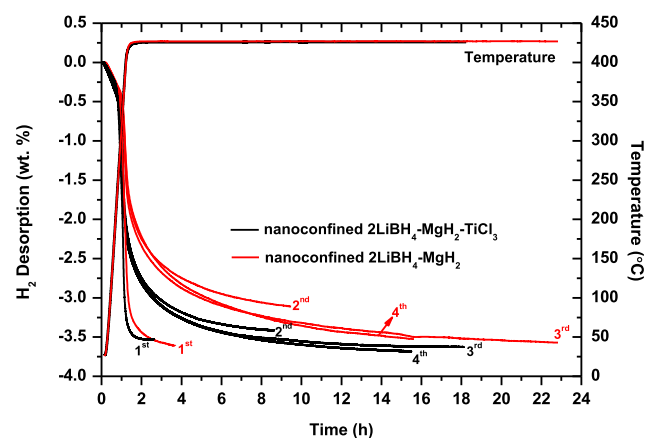Fig. 2 — Coupled manometric—calorimetric analysis of nanoconfined samples of $2LiBH_4$—MgH_2 (A) and $2LiBH_4$—MgH_2—$TiCl_3$ (B).

Fig. 3 — Dehydrogenation profiles and cycling efficiency of nanoconfined samples of $2LiBH_4$—MgH_2 and $2LiBH_4$—MgH_2—$TiCl_3$.

obtained from nanoconfined $2LiBH_4-MgH_2-TiCl_3$, where the total hydrogen content is released approximately twice as fast as the sample without a catalyst. Afterwards, the dehydrogenated samples from the 1st cycle was rehydrogenated at 425 °C under 130 bar H_2. For the 2nd cycles, the superior kinetics and greater amount of hydrogen reproduced are obviously achieved from nanoconfined $2LiBH_4-MgH_2-TiCl_3$. For instance, after 8 h nanoconfined $2LiBH_4-MgH_2-TiCl_3$ releases 3.25 wt. % H_2, while that of nanoconfined $2LiBH_4-MgH_2$ is less than 3 wt. % H_2 (Fig. 3). Due to the inferior amount of hydrogen released in the 2nd cycle as compared with the 1st cycle, the hydrogen pressure during the 2nd rehydrogenation was increased to 145 bar (425 °C). In the 3rd and 4th cycles, nanoconfined $2LiBH_4-MgH_2-TiCl_3$ reveals comparable kinetics and H_2 storage capacity of ∼3.6–3.75 wt. % H_2 after 15 h. With regard to nanoconfined $2LiBH_4-MgH_2$, a similar dehydrogenation phenomenon is also achieved during the 3rd and 4th cycles, where comparable kinetics is obtained. Interestingly, the superior kinetics and H_2 storage capacity are still accomplished during the 3rd and 4th cycles of nanoconfined $2LiBH_4-MgH_2-TiCl_3$, that is, after 14 h, nanoconfined $2LiBH_4-MgH_2-TiCl_3$ releases ∼3.75 wt. % H_2, while that of nanoconfined $2LiBH_4-MgH_2$ is ∼3.4 wt. % H_2 (the 4th cycle in Fig. 3). Thus, it can be concluded from the titration results that the kinetics of nanoconfined $2LiBH_4-MgH_2$ is improved after $TiCl_3$ impregnation in accordance with the coupled manometric–calorimetric results. In this regard, the small amount of $TiCl_3$ (1.6 wt. % with respect to RF–CAS) not only improves significantly the kinetics of the system, but also reproduces the highest H_2 storage capacity after four cycles of 3.6–3.75 wt. % (95–98.6% of theoretical H_2 storage capacity), which is greater than that of the nanoconfined sample without catalyst (∼3.5 wt. % H_2, i.e., 91.4% of theoretical H_2 storage capacity).

To clearly show the influence of $TiCl_3$ on the kinetics of nanoconfined $2LiBH_4-MgH_2$, the normalized hydrogen desorption profiles are considered. From Fig. 4, nanoconfined $2LiBH_4-MgH_2-TiCl_3$ produces the greatest dehydrogenation rate at all cycles over nanoconfined and bulk $2LiBH_4-MgH_2$ samples. It is found that during the 1st and 2nd cycles, nanoconfined $2LiBH_4-MgH_2-TiCl_3$ requires ∼2 and 4.5 h, respectively, to release 95% of the total hydrogen content, while the
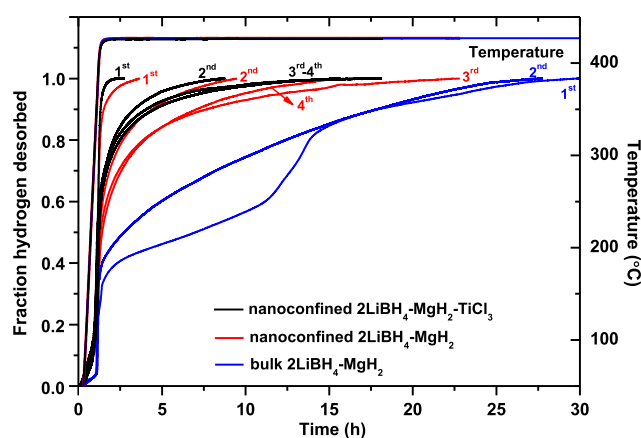
times for nanoconfined $2LiBH_4-MgH_2$ (∼1 and 7 h, respectively) and bulk material (∼23 and 22 h, respectively) are considerably longer. Concerning the ball-milled $2LiBH_4-MgH_2-1$ mol% $TiCl_3$ sample reported elsewhere [12], ∼5 h (at 450 °C) was required to complete 95% of the two-step dehydrogenation. Therefore, nanoconfined $2LiBH_4-MgH_2-TiCl_3$ provides a considerable kinetic improvement at a lower temperature (425 °C) based on the single-step reaction and a five times faster dehydrogenation rate. During the 3rd and 4th cycles, the complete dehydrogenations of nanoconfined $2LiBH_4-MgH_2-TiCl_3$ are accomplished after 17.5 h, while nanoconfined $2LiBH_4-MgH_2$ needs up to 22.5 h (3rd cycle) (Fig. 4). Interestingly, the kinetics of nanoconfined $2LiBH_4-MgH_2-TiCl_3$ seems to be stable after the 3rd cycle, as shown by the overlapped kinetic plots of the 3rd and 4th cycles.

3.4. Reaction mechanisms and reversibility

Reaction mechanisms during each process of nanoconfined $2LiBH_4-MgH_2-TiCl_3$ were investigated by in situ synchrotron radiation powder X-ray diffraction (SR-PXD) and Fourier transform infrared spectroscopy (FTIR). A single scan X-ray diffraction pattern was obtained after each state of melt infiltration, dehydrogenation and rehydrogenation. From Fig. 5(a), the broad region in agreement with a graphite-like structure of RF–CAS is observed in the 2θ range of 10–15° [4,33]. Furthermore, the Bragg diffraction peaks of α-$LiBH_4$, MgH_2, TiB_2, and LiCl, with no presence of $TiCl_3$, are observed. This implies that during melt infiltration $LiBH_4$ partially reacts with all the $TiCl_3$ to produce TiB_2 and LiCl, while MgH_2 does not undergo any reaction. With respect to the SEM–EDS results of nanoconfined $2LiBH_4-MgH_2-TiCl_3$, $TiCl_3$ is completely impregnated in the RF–CAS matrices after melt infiltration, as indicated by significant appearances of Ti and Cl signals (Fig. 1(C) and (D)). Therefore, the reaction between $LiBH_4$ and
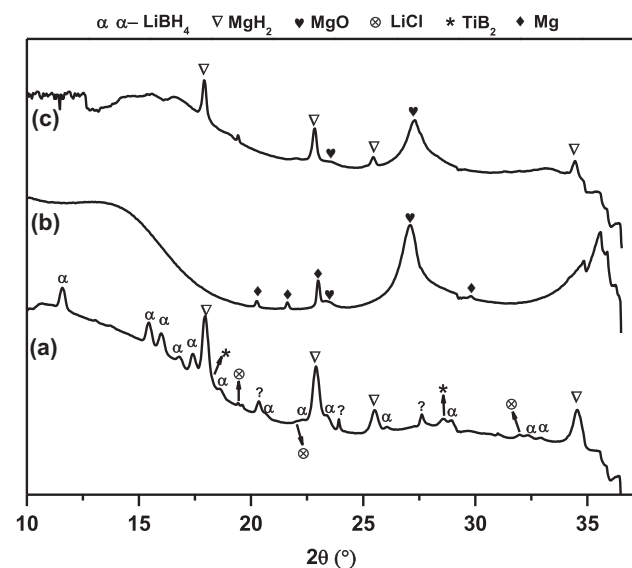

Fig. 4 – Normalized hydrogen desorption profiles of bulk $2LiBH_4-MgH_2$ and nanoconfined samples of $2LiBH_4-MgH_2$ and $2LiBH_4-MgH_2-TiCl_3$.

Fig. 5 – SR-PXD single scans of the nanoconfined $2LiBH_4-MgH_2-TiCl_3$ after melt infiltration (a), after dehydrogenation (b), and after rehydrogenation (c).

$TiCl_3$ (in RF–CAS) confirms the nanoconfinement of $LiBH_4$ in RF–CAS. On the basis of the clear diffraction peaks of $LiBH_4$ and the reaction between $LiBH_4$ and $TiCl_3$, it can be hypothesized that $LiBH_4$ is both on the surface and in the nanopores of RF–CAS after infiltration as in the case of MgH_2. Afterwards, the dehydrogenated sample, obtained from heating the infiltrated sample to 435 °C under 3.5 bar H_2 and keeping it at isothermal and isobaric conditions for 1 h, exhibits the diffraction peaks of Mg and MgO as well as broad region corresponding to the graphite-like structure of RF–CAS (Fig. 5(b)). This suggests the successful dehydrogenation of MgH_2 to Mg. For MgO, it could be due to the oxidation of Mg from a small amount of oxygen in the sapphire capillary. In the case of $LiBH_4$, dehydrogenation is also accomplished, as confirmed by the disappearance of its diffraction peaks as well as the hydrogen content released from titration results (3.6 wt. % H_2). However, the diffraction peaks of the dehydrogenation products (e.g., LiH and MgB_2) cannot be determined due to their complete nanoconfinement in RF–CAS [18]. For rehydrogenation, the dehydrogenated sample was heated to 435 °C (3 °C/min) under 100–120 bar H_2, kept at this temperature for 1 h, and cooled to room temperature. In Fig. 5(c), the diffraction peaks of MgH_2 are presented, together with those of MgO gained during dehydrogenation. In order to conclude that the system is reversible, not only the formation of MgH_2 after rehydrogenation needs to be confirmed, but also the formation of $LiBH_4$ must be established. However, due to the fact that nanoconfined $LiBH_4$ is inactive for X-ray diffraction, no traces of $LiBH_4$ were detected in the diffraction pattern after rehydrogenation. Therefore, an alternative investigation by FTIR was performed. Fig. 6(a) shows the characteristic peaks of commercial $LiBH_4$ infrared absorption at 2390, 2302, 2222, and 1127 cm^{-1} [34,35]. From Fig. 6(b), the rehydrogenated sample of nanoconfined $2LiBH_4$–MgH_2–$TiCl_3$ shows all the characteristic peaks corresponding to pristine $LiBH_4$, as revealed in Fig. 6(a). Thus, the formations of MgH_2 and $LiBH_4$ after rehydrogenation prove the reversibility of nanoconfined $2LiBH_4$–MgH_2–$TiCl_3$ as a hydrogen storage material.
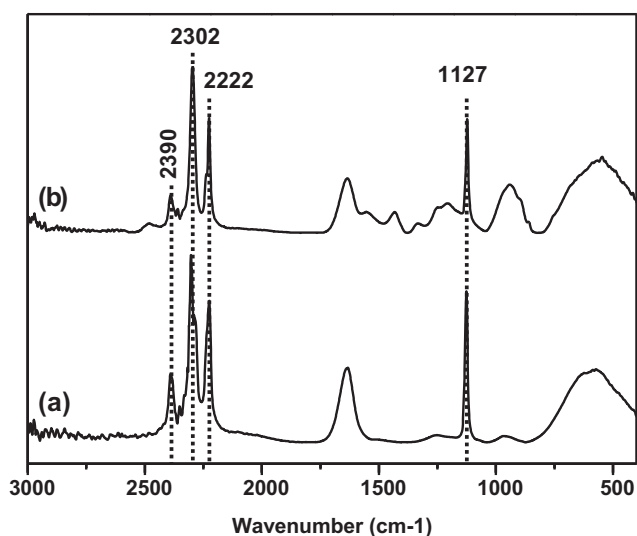

Fig. 6 – FTIR spectra of pristine $LiBH_4$ (a) and nanoconfined $2LiBH_4$–MgH_2–$TiCl_3$ after rehydrogenation (b).

4.   Conclusion

A hydrogen storage material of nanoconfined $2LiBH_4$–MgH_2–$TiCl_3$ was prepared by $TiCl_3$ solution impregnation and $2LiBH_4$–MgH_2 melt infiltration. Nanoconfinement of both $TiCl_3$ and bulk $2LiBH_4$–MgH_2 was confirmed by N_2 adsorption–desorption and SEM–EDS measurements. The reaction mechanisms, revealed by SR-PXD and FTIR experiments, assured the reversibility of this hydrogen storage material. The kinetics improved significantly by adding only 1.6 wt. % $TiCl_3$ (with respect to RF–CAS content) in the nanoconfined $2LiBH_4$–MgH_2. For example, nanoconfined $2LiBH_4$–MgH_2–$TiCl_3$ released total hydrogen within 2 h during the 1st cycle, while nanoconfined and bulk $2LiBH_4$–MgH_2 required 4 and more than 25 h, respectively. Moreover, the hydrogen reproducibility of nanoconfined $2LiBH_4$–MgH_2–$TiCl_3$ after four release and uptake cycles was maintained at 3.6–3.75 wt. % (95–98.6% of theoretical hydrogen storage capacity), which was higher than that of nanoconfined $2LiBH_4$–MgH_2 in the same temperature and time ranges. These results confirmed that the small amount of $TiCl_3$ present in the nanoconfined sample not only improved the kinetics of the system, but it also promoted hydrogen reproducibility after several cycles.

REFERENCES

[1] Fang ZZ, Kang XD, Wang P. Improved hydrogen storage properties of $LiBH_4$ by mechanical milling with various carbon additives. Int J Hydrog Energy 2010;35:8247–52.

[2] Xu J, Cao J, Yu X, Zou Z, Akins DL, Yang H. Enhanced catalytic hydrogen release of $LiBH_4$ by carbon-supported Pt nanoparticle. J Alloys Compd 2010;490:88–92.

[3] Bösenberg U, Doppiu S, Mosegaard L, Berkhordarian G, Eigen N, Borgschulte A, et al. Hydrogen sorption properties of MgH_2–$LiBH_4$ composites. Acta Materialia 2007;55:3951–8.

[4] Gosalawit-Utke R, Nielsen TK, Saldan I, Laipple D, Cerenius Y, Jensen TR, et al. Nanoconfined $2LiBH_4$–MgH_2 prepared by direct melt infiltration into nanoporous materials. J Phys Chem C 2011;115:10903–10.

[5] Gross AF, Vajo JJ, Van Atta SL, Olson GL. Enhanced hydrogen storage kinetics of $LiBH_4$ in nanoporous scaffold. J Phys Chem C 2008;112:5651–7.

[6] Zaluska A, Zaluski L, Ström-Olsen JO. Nanocrystalline magnesium for hydrogen storage. J Alloys Compd 1999;288:217–25.

[7] Lu J, Choi YJ, Fang ZZ, Sohn HY, Rönnebro E. Hydrogen storage properties of nanosized MgH_2–$0.1TiH_2$ prepared by ultrahigh-energy-high-pressure milling. J Am Chem Soc 2009;131:15843–52.

[8] Hao S, Sholl DS. Effect of TiH_2-induced strain on thermodynamics of hydrogen release from MgH_2. J Phys Chem C 2012;116:2045–50.

[9] Yu XB, Grant DM, Walker GS. Dehydrogenation of $LiBH_4$ destabilized with various oxides. J Phys Chem C 2009;113:17945–9.

[10] Mao JF, Wu Z, Chen TJ, Weng BC, Xu NX, Huang TS, et al. Improved hydrogen storage of $LiBH_4$ catalyzed magnesium. J Phys Chem C 2007;111:12495–8.

[11] Yu XB, Grant DM, Walker GS. A new dehydrogenation mechanism for reversible multicomponent borohydride systems – the roll of Li–Mg alloys. Chem Commun 2006;37:3906–8.

[12] Sridechprasat P, Suttisawat Y, Rangsunvigit P, Kitiyana B, Kulprathipanja S. Catalyzed $LiBH_4$ and MgH_2 mixture for hydrogen storage. Int J Hydrog Energy 2011;36:1200–5.

[13] Liu BH, Zhang BJ, Jiang Y. Hydrogen storage performance of $LiBH_4$+$1/2MgH_2$ composites improved by Ce-based additive. Int J Hydrog Energy 2011;36:5418–24.

[14] Gross AF, Ahn CC, Van Atta SL, Liu P, Vajo JJ. Fabrication and hydrogen sorption behavior of nanoparticulate MgH_2 incorporated in a porous carbon host. Nanotechnology 2009;20:204005.

[15] Paskevicius M, Tian HY, Sheppard DA, Webb CJ, Pitt MP, Gray EM, et al. Magnesium hydride formation within carbon aerogel. J Phys Chem C 2011;115:1757–66.

[16] Nielsen TK, Manickam K, Hirscher M, Besenbacher F, Jensen TR. Confinement of MgH_2 nanocluster within nanoporous aerogel scaffold materials. ACS Nano 2009;3:3521–8.

[17] Gao J, Adelhelm P, Verkuijlen MHW, Rongeat C, Herrich M, van Bentum PJM, et al. Confinement of $NaAlH_4$ in nanoporous carbon: impact on H_2 release, reversibility, and thermodynamics. J Phys Chem C 2010;114:4675–82.

[18] Gosalawit-Utke R, Nielsen TK, Pranzas K, Saldan I, Pistidda C, Karimi F, et al. $2LiBH_4$–MgH_2 in a resorcinol–furfural carbon aerogel scaffold for reversible hydrogen storage. J Phys Chem C 2011;116:1526–34.

[19] Nielsen TK, Bösenberg U, Gosalawit R, Dornheim M, Cerenius Y, Besenbacher F, et al. Reversible nanoconfined chemical reaction. ACS Nano 2010;4:3903–8.

[20] Mulas G, Campesi R, Garroni S, Napolitano E, Milanese C, Dolci F, et al. Hydrogen storage in $2NaBH_4$–MgH_2 mixtures:

destabilization by additives and nanoconfinement. J Alloys Compd 2012;536:S236–40.

[21] Lee HS, Lee YS, Suh JY, Kim M, Yu JS, Cho YW. Enhanced desorption and absorption properties of eutectic $LiBH_4$–$Ca(BH_4)_2$ infiltrated into mesoporous carbon. J Phys Chem C 2011;115:20027–35.

[22] Nielsen TK, Polanski M, Zasada D, Javadian P, Besenbacher F, Bystrzycki J, et al. Improved hydrogen storage kinetics of nanoconfined $NaAlH_4$ catalyzed with $TiCl_3$ nanoparticles. ACS Nano 2011;5:4056–64.

[23] Bösenberg U, Vainio U, Pranzas PK, von Colbe JMB, Goerigk G, Weiter E, et al. On the chemical state and distribution of Zr- and V-based additives in reactive hydride composites. Nanotechnology 2009;20:204003.

[24] Deprez E, Munoz-Marquez MA, Roldan MA, Prestipino C, Palomares FJ, Minella CB, et al. Oxidation state and local structure of Ti-based additives in the reactive hydride composite $2LiBH_4$–MgH_2. J Phys Chem C 2010;114:3309–17.

[25] Fan MQ, Sun LX, Zhang Y, Xu F, Zhang J, Chu HL. The catalytic effect of additive Nb_2O_5 on the reversible hydrogen storage performance of $LiBH_4$–MgH_2 composite. Int J Hydrog Energy 2008;33:74–80.

[26] Li WC, Lu AH, Weidenthaler C, Schüth F. Hard-templating pathway to create mesoporous magnesium oxide. Chem Mater 2004;16:5676–81.

[27] Halsey G. Physical adsorption on non-uniform surfaces. J Chem Phys 1948;16:931–8.

[28] de Boer JH, Linsen BG, Plas Th, Zondervan GJ. Studies on pore systems in catalysts: VII. Description of the pore dimension of carbon blacks by the t method. J Catal 1969;4:649–53.

[29] Brunauer S, Emmet P, Teller E. Adsorption of gases in multimolecular layers. J Am Chem Soc 1939;60:309–19.

[30] Barrett EP, Joyner LG, Halenda PP. The determination of pore volume and area distributions in porous substances. I. Computations from nitrogen isotherms. J Am Chem Soc 1951;73:373–80.

[31] Cerenius Y, Ståhl K, Svesson LA, Ursby T, Oskarsson Å, Albertsson J, et al. The crystallography beamline I711 at MAX II. J Synchrotron Rad 2000;7:203–8.

[32] Yan Y, Li HW, Maekawa H, Miwa K, Towata S, Orimo S. Formation of intermediate compound $Li_2B_{12}H_{12}$ during the dehydrogenation process of the $LiBH_4$–MgH_2 system. J Phys Chem C 2011;115:19419–23.

[33] Li J, Wang X, Huang Q, Gamboa S, Sebastian PJ. Studies on preparation and performances of carbon aerogel electrodes for the application of supercapacitor. J Power Sources 2006;158:784–8.

[34] Wan X, Shaw LL. Novel dehydrogenation properties derived from nanoscale $LiBH_4$. Acta Materialia 2011;59:4606–15.

[35] Wu X, Wang X, Cao G, Li S, Ge H, Chen L, et al. Hydrogen storage properties of $LiBH_4$–Li_3AlH_6 composites. J Alloys Compd 2012;517:127–31.